Enhanced Ocean Wave Modeling by Including Effect of Breaking under Both Deep- and Shallow-Water Conditions

Yue Xu[1] and Xiping Yu[2]

[1] Department of Hydraulic Engineering, Tsinghua University, Beijing, China.

[2] Department of Ocean Science and Engineering, Sothern University of Science and Technology, Shenzhen, China.

Correspondence to: Xiping Yu (yuxp@sustech.edu.cn)

Abstract

Accurate description of the wind energy input into ocean waves is crucial to ocean wave modeling and a physics-based consideration on the effect of wave breaking is absolutely necessary to obtain such an accurate description. This study evaluates the performance of an improved formula recently proposed by Xu and Yu (2020), who took into account not only the effect of breaking but also the effect of air-flow separation on the leeside of steep wave crests in a reasonably consistent way. Numerical results are obtained through coupling an enhanced atmospheric wave boundary layer model with the ocean wave model WaveWatch III (v5.16). The coupled model has been extended to be valid in both deep and shallow waters. Duration-limited waves under controlled normal conditions and storm waves under practical hurricane conditions are studied in details to verify the improved model. Both the representative wave parameters and the parameters characterizing the wave spectrum are discussed. It is shown that the improved source-term package for the wind energy input and the wave energy dissipation leads to more accurate results under all conditions. It performs evidently better than other standard source-term options of ST2, ST4 and ST6 embedded in WaveWatch III. It is also demonstrated that the improvement is particularly important for waves at their early development stage and waves in shallow waters.

Keywords: Source-term option; Breaking effect; Atmospheric wave boundary layer model; WaveWatch III; Duration-limited waves; Hurricane-generated waves.

1. Introduction

Accurate modeling of ocean waves depends straightforwardly on a correct formulation of the wind energy supply to the waves through the ocean surface as well as the wave energy dissipation within the ocean surface layer, and eventually on a thorough understanding to the physics underlying these two dynamic processes. The wind energy input supports the generation and growth of ocean waves, while the wave energy dissipation always occurs owing not only to the viscous property of the fluid but also to the effects of turbulent mixing and multiphase interaction that take place in the boundary layer at both sides of the air-sea interface. In the past decades, a tremendous number of research efforts have been made to enhance our understanding on the phenomena of wind energy input into ocean waves and the dissipation of ocean surface waves due to various mechanisms (Janssen, 1989; 1991; 2004; Hasselmann et al., 1973; Snyder et al., 1981; Donelan et al., 2006; Babanin et al., 2007; Ardhuin et al., 2010; Rogers et al., 2012). However, a comprehensive integration of the accumulated knowledge, particularly those developed under extreme conditions in shallow waters, does not seem to have been satisfactorily achieved up to date.

Janssen (1989; 1991; 2004) proposed the most classical formula for the wind energy input based on the resonance theory of Miles (1957; 1965), in which the wind drag as a deterministic function of the roughness height of the ocean surface is a critical parameter. Hasselmann et al. (1973) obtained an expression for the wind energy input by solving the wave energy equation and then calibrating parameters with field data from the joint North Sea wave project (JONSWAP). Snyder et al. (1981) and Donelan et al. (2006) conducted field experiments in the Bight of Abaca, Bahamas, and Lake George, Australia, and included more physics in their formula for the wind energy input. Badulin et al. (2007) and Zakharov et al. (2012; 2017) proposed a new method to establish a theory for the wind energy input by considering the weakly turbulent law for wind-wave growth. In spite of these important achievements, the wind energy input is still not yet satisfactorily formulated, basically due to complexity of the phenomenon as well as the physics underlying the phenomenon.

Researchers have found substantial differences between wind energy input through

ocean surfaces with and without wave breaking (Banner and Melville, 1976). Data collected during the AUSWEX field campaign at Lake George, Australia (Babanin et al., 2007) showed that under a severe breaking condition, the wind energy input will increase to about 2 times of that under a relevant non-breaking condition. Although the important effects of wave breaking as well as short-wave dissipation on wind energy input have been well understood (Janssen, 1989, 1991; Makin and Kudryavtsev, 1999; Hasselmann et al., 1973; Babanin et al., 2007), it is only until recent that Xu and Yu (2020) proposed a formula to effectively include these effects. Xu and Yu (2020)'s formula takes into consideration both the breaking effect and the effect of air-flow separation on the leeside of steep wave crests in a reasonably consistent way. Despite of its physics-based nature, a further evaluation of its performance in practical and more complicated wind wave conditions, however, is still necessary.

It is generally believed that, among the total wind energy transferred into the ocean waves, a part is absorbed by the long-wave components to support wave growth while an even larger part is received by the short-wave components and quickly dissipated due to fluid viscosity, wind shear on the ocean surface and the turbulence effect related to wave breaking (Csanady, 2001; Jones and Toba, 2001). Formulation of the wave dissipation, however, is very difficult and the available suggestions in the literature are rather controversial (Cavaleri et al., 2007). The earliest wave dissipation model is known to be the probabilistic breaking model originally presented by Longuet-Higgins (1969) and then improved by Yuan et al. (1986). Hasselmann (1974) proposed the whitecap model based on a mathematical formulation of the negative work done by the downward whitecap pressure on the upward wave motion. Phillips (1985) and Donelan and Pierson (1987) proposed the quasi-saturation model by assuming a local equilibrium relationship among wind energy input, nonlinear transfer and wave dissipation. Polnikov (1993) preferred the turbulence dissipation model which relates the loss of wave energy to the dissipation of turbulence kinetic energy. In addition to the theoretical studies, a significant number of experimental investigations have also been carried out (Phillips et al., 2001; Melville and Matusov, 2002; Donelan, 2001; Hwang, 2005). Based on the data measured at Lake George, Australia,

Bananin and Young (2005) established an empirical model, in which the concept of cumulative effect is introduced so that the contribution of low-frequency wave motion to breaking of high-frequency waves can be taken into account. It may be necessary to point out that most of the experimental studies are supported only by limited data.

WaveWatch III (WWIII), a successful third-generation wave model, has been widely used for simulating ocean waves in both deep and shallow waters. With great efforts made by scientists around the world (Ardhuin et al., 2010; Zieger et al., 2015), parameterizations of the source terms in WWIII have been well calibrated under various conditions to achieve satisfactory results for evolution of an ocean wave spectrum. Under severe wave conditions, however, their accuracy is often unsatisfactory and the wave energy is underestimated even with an optimal choice of the parameters (Cavaleri et al., 2020; Campos et al., 2018; Mentaschi et al., 2015). Meanwhile, researchers found that the directional wave spectrum has been sometimes very poorly simulated even when the significant wave parameters are accurately represented (Fan and Rogers, 2016). Stopa et al. (2016) believed that all wave models have difficulty in describing the directional spread of waves. Although modelers usually tend to attribute the numerical error to the inaccuracy of the wind data or topography data, we must admit that imperfection of the source term parameterization, especially under severe wave conditions, is also one of the main reasons.

In this study, improved formulas for the wind energy input and the wave energy dissipation are embedded into the WWIII version 5.16, though it may also be applied to other ocean wave models. The enhanced atmospheric wave boundary layer model (AWBLM) (Xu and Yu, 2021) is also coupled to ensure a more accurate wind stress evaluation at high wind speed and in finite water depth. The performances of the improved formulas are evaluated under both idealized wind conditions and real extreme conditions. Attention is also paid to their differences in deep- and shallow-waters. The structure of the paper is arranged as follows. The improved formulation as well as the framework of the coupled AWBLM-WWIII model are described in Section 2. Model verification under controlled conditions is presented in Section 3, while model verification under extreme wind conditions is presented in Section 4. Section 5 is a summary of conclusions.

2. Model Description

2.1 Coupled AWBLM-WWIII Model

The ocean wave model WaveWatch III numerically solves the energy conservation equation for wave action density spectrum (WW3DG, 2016):

$$\frac{DN}{Dt} = \frac{S}{\omega} \tag{1}$$

$$S = S_{\text{in}} + S_{\text{ds}} + S_{\text{nl}} \tag{2}$$

where $N\ \omega,\theta$ is the wave action density spectrum; ω is the relative frequency; S is the source/sink term given by Eq. (2). In general, the source term S must represent three different mechanisms: the wind energy input into waves S_{in}, the wave energy dissipation S_{ds}, the nonlinear wave-wave interaction S_{nl}. Although S_{in} and S_{ds} represent different physical processes, they should be considered and calibrated interrelatedly since the net effect of these two sources rather than each of them can be more accurately measured on many occasions and it is the net effect that governs the growth/decay of the ocean waves. S_{nl} plays a key role in the evolution of wave spectrum shape and may, at least theoretically, be evaluated through correctly solving the nonlinear transfer integrals. Note that, in shallow waters, the wave energy dissipation must include those due to bottom friction and depth-induced breaking, denoted by S_{dsf} and S_{dsb}, respectively, in addition to that due to whitecaps, denoted by S_{dsw}, i.e., $S_{\text{ds}} = S_{\text{dsf}} + S_{\text{dsb}} + S_{\text{dsw}}$. It may also be worthwhile mentioning that an accurate evaluation of the nonlinear interaction effect is surprisingly difficult for the high-frequency wave components, particularly in shallow waters. Therefore, it is frequently suggested to apply a semi-empirical theory for evaluating S_{nl}, i.e., let $S_{\text{nl}} = S_{\text{nl4}} + S_{\text{nl3}}$, where S_{nl4} and S_{nl3} are expressed as functions of the wave frequency as well as the wave direction, and represent the quartet and triad wave interactions, which play dominant roles in deep and shallow waters, respectively.

In order to accurately simulate ocean waves under moderate to severe wind conditions, and from deep to shallow water conditions, an advanced atmospheric wave boundary layer model (AWBLM) must be coupled into WWIII for a dynamic evaluation of the wind stress.

The AWBLM applicable for this purpose is well described in Xu and Yu (2021), which may take effects of both ocean surface state and water depth into consideration, and has certain advantages compared to a simple quadratic formula for the wind stress. In the coupled model, the source terms are treated in the following way. Quartet-wave interaction is computed with the standard discrete interaction approximation (DIA). Note that, though it may bring some uncertainty into the numerical results for nonlinear effects, the DIA method is still widely employed in practical applications due to its minimum requirement on the computational efforts (Liu et al., 2017; Stopa et al., 2015; Ardhuin et al., 2010). Triad-wave interaction is evaluated with the Lumped Triad Approximation model (Eldeberky, 1996). The bottom friction effect is described by the simple model of JONSWAP (Hasselmann et al., 1973). The Battjes and Janssen (1978) parameterization is employed to represent the effect of depth-induced breaking. The parameters included in all source terms except for those with special emphases follow the default setting. The wind energy input and the wave energy dissipation are considered as a package in this study. WWIII provides four typical options of this package, i.e., ST2, ST3, ST4, ST6, among which ST3 and ST4 are based on the same formulation of Janssen (2004) for the wind energy input. Since ST4 has been frequently reported to have a better performance than ST3 (Stopa et al., 2016; Beyá et al., 2017; Liu et al., 2017), the ST3 option is neglected in this study. The standard options are carefully compared with the improved model proposed by the present authors (Xu and Yu, 2020).

2.2 Improved Model of Xu and Yu (2020)

The wind energy input in the improved model of Xu and Yu (2020), hereafter referred as ST-XY option, is expressed by

$$S_{\mathrm{in}}\ k,\theta\ = \frac{\rho_{\mathrm{a}}}{\rho_{\mathrm{w}}}\omega\gamma_{\mathrm{g}}\ k,\theta\ E\ k,\theta \tag{3}$$

$$\gamma_{\mathrm{g}}\ k,\theta\ = a\left[b_{\mathrm{T}}\lambda G' + \ 1-b_{\mathrm{T}}\ G\right]W^2\sqrt{B_{\mathrm{n}}} \tag{4}$$

$$W = \max\left(0, \frac{U_{10}}{c_{\mathrm{p}}}\cos\ \theta-\theta_{\mathrm{a}}\ -1\right) + a_0\min\left(0, \frac{U_{10}}{c_{\mathrm{p}}}\cos\ \theta-\theta_{\mathrm{a}}\ -1\right) \tag{5}$$

$$B_{\mathrm{n}}\ k\ = A\ k\ \int_{0}^{2\pi} k^{3}E\ k,\theta'\ d\theta' \tag{6}$$

$$b_{\mathrm{T}}\ k\ = 89.5\ \sqrt{B_{\mathrm{n}}\ k\ } - 0.0223^{\ 2} \tag{7}$$

$$G = 2.8 - 1.0\left\{1 + \tanh\left[10\sqrt{B_{\mathrm{n}}}\left(\frac{U_{10}}{c_{\mathrm{p}}}\cos\ \theta - \theta_{\mathrm{a}}\ - 1\right)^{2} - 11\right]\right\} \tag{8}$$

where ρ_{a} is the density of air; ρ_{w} is the density of water; ω is radian frequency; k is the wavenumber, which is related to ω through the dispersion relation; θ is the wave direction; $E\ k,\theta$ is the directional wave energy spectrum; $\gamma_{\mathrm{g}}\ k,\theta$ is the wave growth rate; c_{p} is the celerity of the wave with peak frequency; U_{10} is the wind speed at the 10 m level above the ocean surface; θ_{a} is the wind directon. Note that the basic form of Eq. (3) follows the conventional assumption that S_{in} is propotional to the directional wave spectrum. However, the most crucial factor in S_{in}, i.e., the wave growth rate γ_{g} is formulated to represent the effect of various physical processes. Although γ_{g} is essentially governed by the relative wind speed and the mean steepness of the surface waves, it is considered to be essentially different when wave breaking does or does not occur, and is thus expressed as a weighted average of the different multipliers corresponding to breaking and non-breaking conditions with the breaking probability b_{T} being the weight. The relative wind speed is expressed by Eq. (5), where deflection of the wind direction from the wave direction is fully considered. It may be necessary to point out that the contribution of the inverse wind to energy input is reduced by a factor of $a_{0} = 0.45$ following Liu et al. (2017). Under the non-breaking condition, a separation coefficient G is introduced to represent the 'shelter effect' due to airflow seperation at the lee side of high wave crests following Donelan et al. (2006). When wave breaks, the 'shelter effect' disappears and G reduces to its maximum value $G' = 2.8$. Since wave breaking has an effect of intensifying wind energy input, we introduce an amplification factor λ, and let $\lambda = 2.0$, also following previous studies. It may also be necessary to mention that the wave steepness is related to the satuarated wave spectrum $B_{\mathrm{n}}\ k\ $, as expressed by Eq. (6), where $A\ k\ $ is a

measure of the directional spectrum width. In general, the wind energy input is positive, but it may become negative when a strong swell is in presence and the wind speed is smaller than the wave celerity or when the direction of wind is significantly deflected from the wave direction.

The advantage of the wind energy input in the improved model of Xu and Yu (2020) is its direct representation of the underlying physics. Based on the field observations of both Donelan et al. (2006) and Babanin et al. (2007), the wind energy input into waves under severe conditions is a very complicated process, since random waves may break and may not break depending on the instantaneous local wave steepness. For non-breaking waves, air-flow separation occurs on the leeside of wave crests, and the wind energy input reduces. For breaking waves, the wind energy input is significantly larger due to breaking induced mixing. The improved model of Xu and Yu (2020) fully considers these two effects and, consequently, should be more suitable for the description of severe waves.

Since the ocean wave development depends actually on the net energy gain in the ocean surface layer and it is sometimes very difficult to identify if some amount of wind energy is transferred into the ocean waves and then dissipated or it is dissipated within the atmospheric boundary layer and not received by the ocean at all, S_{in} and S_{ds} must then be considered as a package. In other words, formulation of the dissipation term should be based on a relevant definition of the wind energy input. In this study, we follow the wave dissipation model of Ardhuin et al. (2010) for the whitecap effect. The semi-empirical dissipation model of Ardhuin et al. (2010) can be expressed as (see also Leckler et al., 2013)

$$S_{\mathrm{dsw}} = S_{\mathrm{dsn}} + S_{\mathrm{dsc}} \tag{9}$$

$$S_{\mathrm{dsn}} = \xi_{\mathrm{n}} B_{\mathrm{r}}^{-2} \omega \left[\delta_{\mathrm{d}} \max\left[B\left(k\right) - B_{\mathrm{r}}, 0\right]^2 + \left(1-\delta_{\mathrm{d}}\right) \max\left[B'\left(k,\theta\right) - B_{\mathrm{r}}, 0\right]^2 \right] E\left(k,\theta\right) \tag{10}$$

$$S_{\mathrm{dsc}} = -1.44\xi_{\mathrm{c}} \left\{ \int_0^{r_{\mathrm{c}}k} \int_0^{2\pi} \max\left[\sqrt{B\left(k',\theta'\right)} - \sqrt{B_{\mathrm{r}}}, 0\right]^2 \Delta c_{\mathrm{p}} d\theta' dk' \right\} E\left(k,\theta\right) \tag{11}$$

where, ξ_{n} and ξ_{c} are empirical constants; δ_{d} is a factor introduced to weight the isotropic part and direction-dependent part; r_{c} is the minimum ratio of the wavenumber

that will wipe out the short waves. The saturation spectrum $B_{\mathrm{n}}(k)$ is defined in the same way as before and the directional saturation spectrum $B_{\mathrm{n}}'(k,\theta)$ is defined by

$$B'(k,\theta) = \int_{\theta-\Delta_\theta}^{\theta+\Delta_\theta} k^3 \cos^2(\theta-\theta') E(k,\theta') d\theta' \tag{12}$$

The threshold of $B_{\mathrm{n}}(k)$ is denoted by B_{r}. Note that Eqs. (9), (10) and (11) are based the assumption that wave dissipation consists of an inherent effect and a cumulative effect, both are propotional to the directional wave spectrum. In shallow waters, dissipations due to bottom friction and depth-induced breaking are formulated following Xu and Yu (2021).

2.3 Standard Models

Known reliable formulas for the wind energy input and the wave energy dissipation have been embedded in WWIII. Among all, the following options, which have been widely preferred on different occasions, are chosen for comparison in this study.

(1) ST2 option. This package, originally proposed by Tolman and Chalikov (1996), consists of the wind energy input formula of Chalikov and Belevich (1993) and Chalikov (1995) as well as a relevant wave energy dissipation model. The dissipation model emphasizes the different mechanisms of dissipation for low- and high-frequency waves. The expression for low-frequency waves is based on an analogy to energy dissipation due to turbulence, while that for high-frequency waves is purely empirical. A linear combination of these two expressions then represents the total dissipation. It has been reported that this wind energy input formula may need to be filtered using a special technique when a strong swell is in presence (Tolman, 2002). For the purpose of comparison, the default setting of parameters in this study follows Tolman (2002), who selected this package in WWIII for a global ocean wave modeling and obtained satisfactory results.

(2) ST4 option. This package consists of the wind energy input formula of Janssen (2004), which is based on the wave growth theory of Miles (1957), and the wave energy dissipation model of Ardhuin et al. (2010). The dissipation model appears as the summation of an inherent part and a cumulative part. All parameters are determined following Ardhuin et al. (2010).

(3) ST6 option. This package consists of the formulas for wind energy input and wave

energy dissipation due to whitecaps which fit the field data obtained at Lake George, Australia (Donelan et al., 2006; Rogers et al., 2012). A sink term due to negative wind energy input is considered for inverse winds. The dissipation due to whitecaps is expressed as the sum of an inherent part, which is proportional to wave spectrum, and a cumulative part in terms of the integral properties of the wave spectrum below a certain value of the wavenumber.

3. Model Verification under Controlled Normal Conditions

3.1 Duration-limited waves in deep waters

The ideal problem of wave development over the open sea of infinite water depth is considered. At a given duration, evolution of the directional wave spectrum is simulated with WWIII considering different choices of the source-term package. The uniform wind speed at the 10 m height above ocean surface is fixed at a moderate level of 10 m/s. Sensitivity of the numerical results to the computational time step is also studied. It is shown that a spatial resolution of 1/30° is reasonably accurate for duration-limited wave simulations and a finer grid does not lead to any significant change of the numerical results. The boundary effect in the numerical results is minimized in this case by setting open boundary conditions surrounding a large-enough computational domain. It is also demonstrated that little difference of the numerical results can be observed as the computational time step takes 30 s, 1 min and 10 min. Therefore, the results obtained with the time step equal to 10 min are presented in the remaining part of this study.

In Figure 1, the wave growth curve, i.e., the relationship between the normalized total wave energy ε and the normalized duration τ, computed with different options for the source terms, is presented and compared with the empirical results available in the literature. The four empirical growth curves correspond to Stewart's (1961) law, which was originally presented as tabulated data, Sanders' (1976) law, the CERC (1977) law and Kahma and Calkoen's (1992) law. The equilibrium value given by the Pierson-Moskowitz spectrum (Pierson and Moskowitz, 1964), i.e., $\varepsilon_{\mathrm{PM}} = 3.6 \times 10^{-3}$, as well as the tabulated values of Moskowitz (1964) are also plotted.

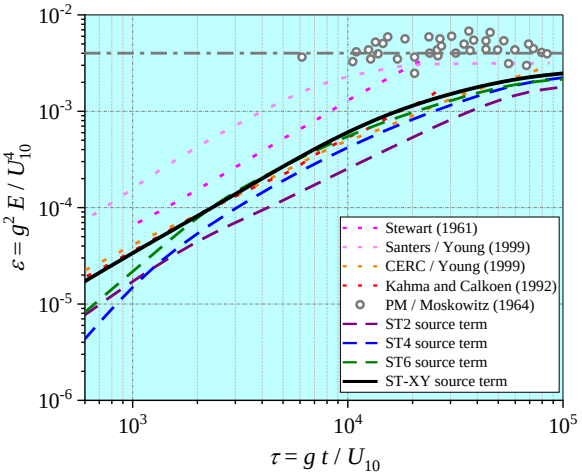

Figure 1. Comparisons of duration-limited growth rate between empirical and computational results. Both wave energy and duration are nondimensionalized with U_{10}

By comparing the computed wave growth curves with each other and with the empirical results as well, it becomes clear that, the WWIII model results with different choices of the source-term package are all rather close to the CERC (1977) law and Kahma and Calkoen's (1992) law, and also agree with the results of Rogers et al. (2012). At a younger wave age, particularly at $\tau < 2\times10^3$, the ST-XY option performs much better while other source-term options underestimate the wave energy significantly. The ST4 option most severely underestimate the wave energy at the early stage of wave development. As duration increases, the results of the ST6 option approaches those of the ST-XY option. When approaching the equilibrium stage ($10^4 < \tau < 10^5$), the numerical results corresponding to ST-XY, ST6 and ST4 options all approach the Pierson-Moskowitz limit while the ST2 option still underestimate the wave energy. In general, the performance of the ST-XY option is obviously better.

Since the source terms are often formulated in terms of the mean wave parameters, evolution of the wave spectrum and development of the mean wave parameters are thus interdependent. Therefore, a comparison of the mean wave parameters obtained with different choice of the source term options, as presented in Figure 2, is highly meaningful. It is demonstrated that the significant wave height H_s and the mean wavelength L_m obtained with the ST-XY option are slightly greater than the results obtained with other options while the ST2 option yields the smallest values. The numerical result of the mean wave period T_{02}

obtained with the ST-XY option is the largest at the early wave development stage, but it becomes almost the same as that obtained with the ST4 option at the equilibrium stage. The mean wave period T_{02} obtained with the ST2 option is the smallest at the early wave-development stage while that obtained with the ST6 option becomes smallest at the equilibrium stage. The peak frequency f_p obtained with ST4, ST6 and ST-XY options is very close to each other, but the ST2 option results in a larger value.

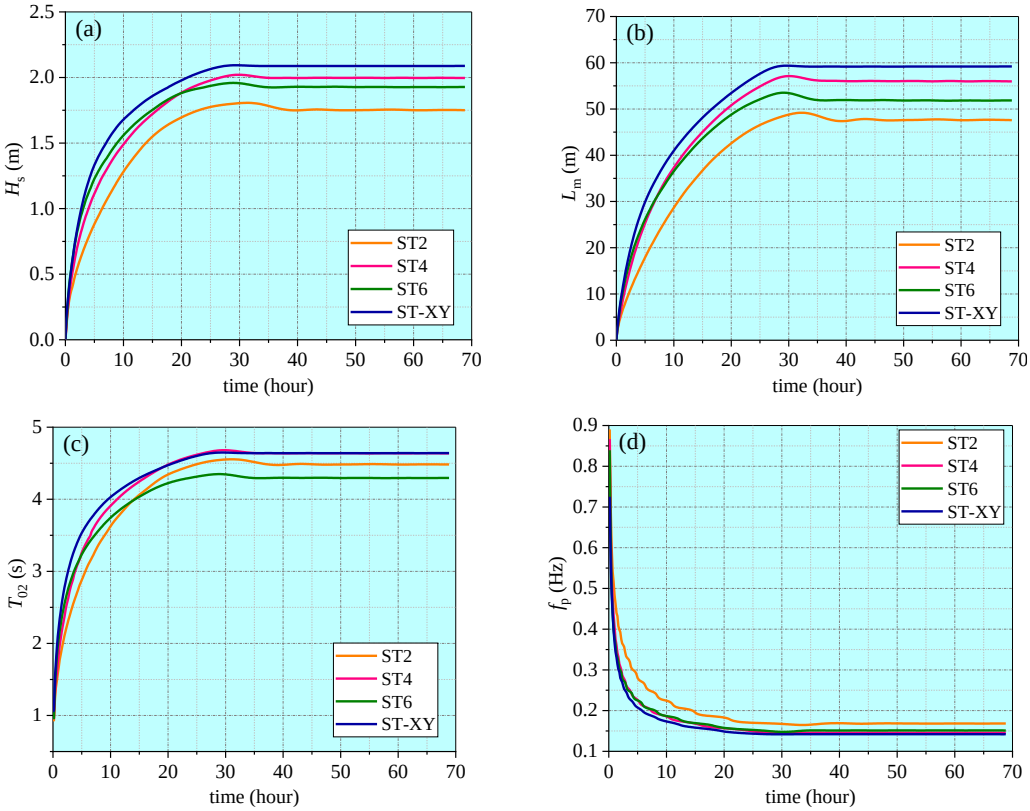

Figure 2. Comparisons of numerical results for (a) significant wave height H_s, (b) mean wave length L_m, (c) mean wave period T_{02} and (d) peak frequency f_p, obtained with different choices of the source-term options.

A comparison of the computed spectra of the wind energy input and the wave energy dissipation with different choices of the source-term options is presented in Figure 3. Note that the spectra obtained with the ST2 option are not presented since they are obviously underestimated. The numerical results strongly indicate that the wind energy input and the wave energy dissipation resulted from the same source-term package are correlated, not only in terms of the peak values but also in terms of the spectral shapes. It is seen that, the

wind energy input resulted from the ST-XY option maintains at a higher level than those resulted from other options at the early wave-development stage, leading to a faster wave growth and higher level of the wave energy at younger wave ages. Relatively concentrated unimodal distributions for both the wind energy input and the wave energy dissipation are built at the early wave-development stage, no matter which source-term option is adopted. As wave development continues, however, the peak frequencies as well as the peak values of the spectra decrease while more wind energy is transferred to the higher frequency waves and bimodal distributions are formed. At this stage, the peak value of the spectra obtained with the ST-XY option is similar to those obtained with the ST6 and ST4 option, while its high-frequency part has higher values than those resulted from the ST6 and ST4 options. When approaching the fully-developed stage, the wind energy input obtained with the ST-XY and ST4 options reaches a peak at relatively low frequency, but the peak obtained with the ST6 option appears at a much higher frequency. This is related to whether the breaking effect is fully considered when formulating the wind energy input.

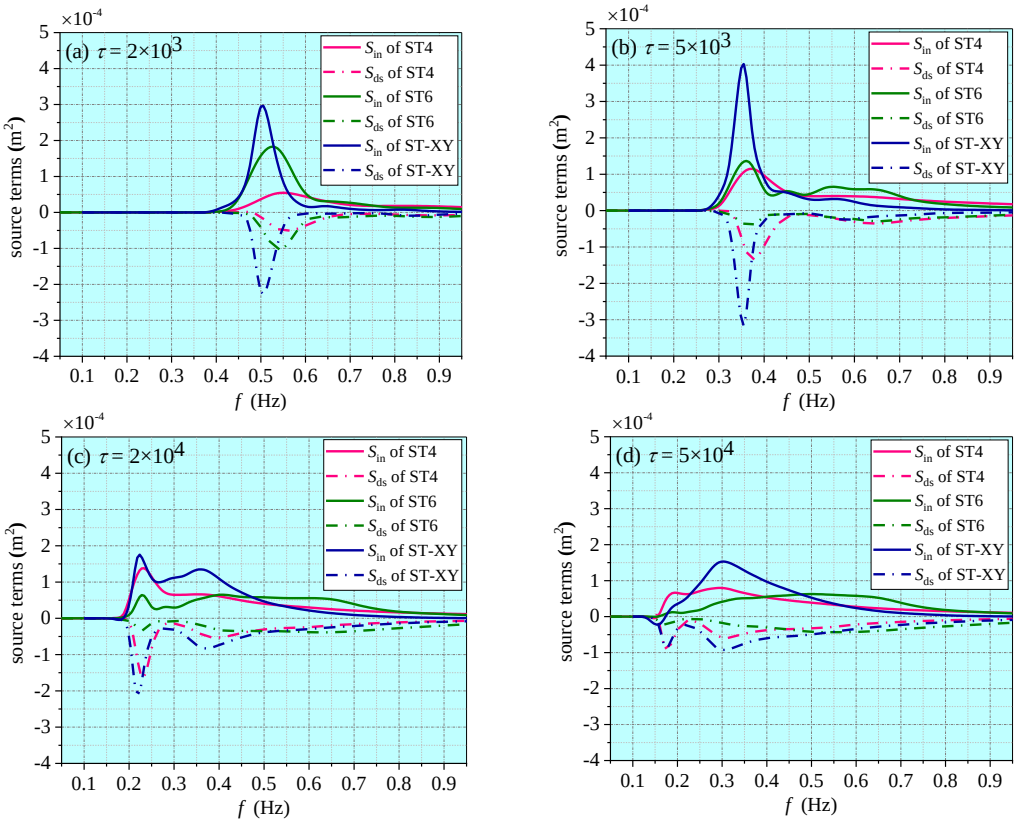

Figure 3. Spectra of the wind energy input and the wave energy dissipation obtained with different choices of the source-term package.

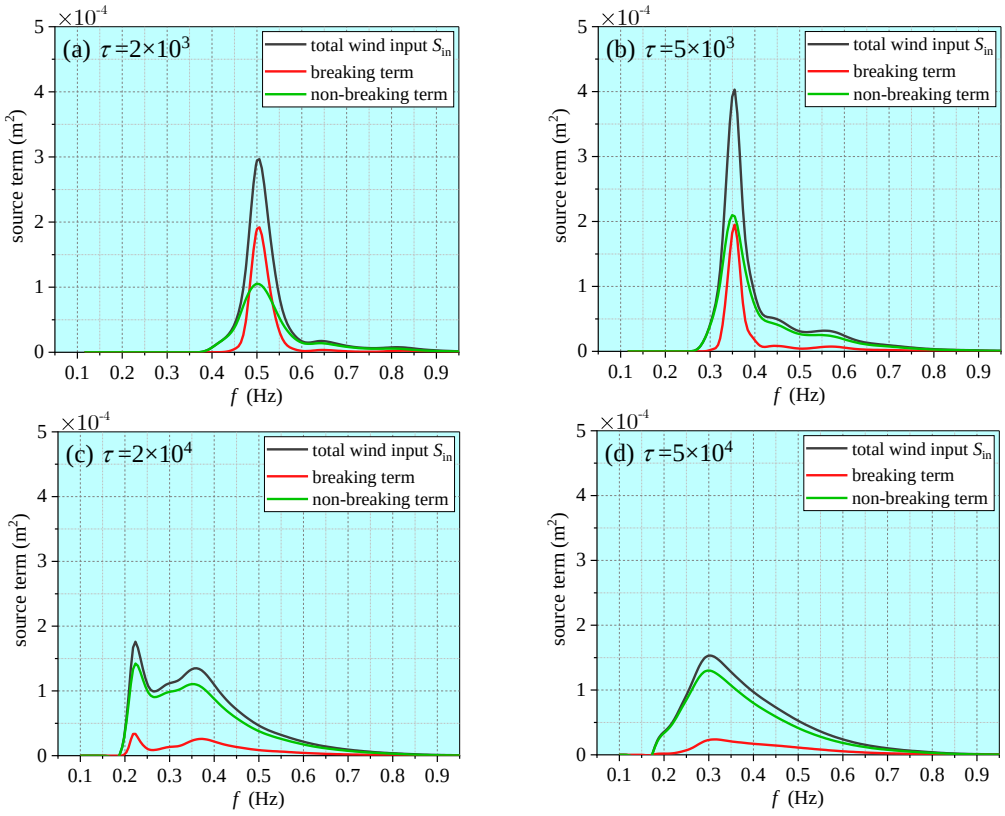

Figure 4. Deepwater spectra of wind energy input under breaking and non-breaking conditions at different wave development stages given by the ST-XY source-term option

A major merit of the improved formula for the wind energy input of Xu and Yu (2020) is the inclusion of breaking effect and the effect of airflow separation on the leesides of steep waves. Among the total wind energy input, the portions taking place under breaking and non-breaking conditions, given by the improved formula of Xu and Yu (2020), are presented in Figure 4. It is clearly demonstrated that, at the early wave-development stage, over 60% of the peak wind energy input takes place under the breaking condition. As wave development continues, the proportion of the peak wind energy input under breaking conditions decreases rapidly. When approaching the equilibrium stage, only 15% of the peak wind energy input happens under breaking conditions. The trend suggested by our numerical results is in very good agreement with the facts reported in previous studies (Janssen, 1989; Hasselmann et al., 1973). Field observations indicate that wind energy input into breaking waves is about 2 times larger than that into non-breaking waves (Donelan et al., 2006; Babanin et al., 2007). Because of a relatively large amount of wind energy input into the breaking wave components in the early wave-development stage, one observes a

faster wave growth and higher level of the wave energy at younger wave ages. It is thus reasonable to conclude that the ST-XY option for the wind energy input and the wave energy dissipation successfully integrated the known information about the effect of breaking on the wind energy input and improved the performance of the WWIII model, especially at the early wave-development stage when the wave energy has often been underestimated.

3.2 Duration-limited waves in shallow waters

In order to evaluate its performance in nearshore environment, the ST-XY source-term option is also applied to the simulation of duration-limited waves in shallow waters. The computational conditions are the same as those adopted in the deep-water case except for a varying water depth from 5 m to 1 m. The nondimensional water depth $\delta = gd/U_{10}^2$ then varies from 0.5 to 0.1. The computational results are compared with field observations of Young and Verhagen (1996), who systematically measured the variations of wave parameters and wave spectrum in shallow waters. Since the measured data was provided in a fetch-limited manner, the method of Hwang and Wang (2004) is used to transfer the duration-limited numerical results to fetch-limited ones for comparison. As demonstrated in Figure 5, the numerical results obtained with the ST-XY source-term option in shallow waters match well with the field data. As the nondimensional water depth increases from 0.1 to 0.5, the wave energy increases while the peak frequency decreases. This is well explained by the effect of water depth on wave steepness and wave height. Within each range of the water depth, the field data basically fall into the relevant two curves resulted from the model. This is particularly accurate for the wave energy. Therefore, it may be concluded that the improved source-term option of Xu and Yu (2020) is also effective for ocean wave modeling under shallow water conditions.

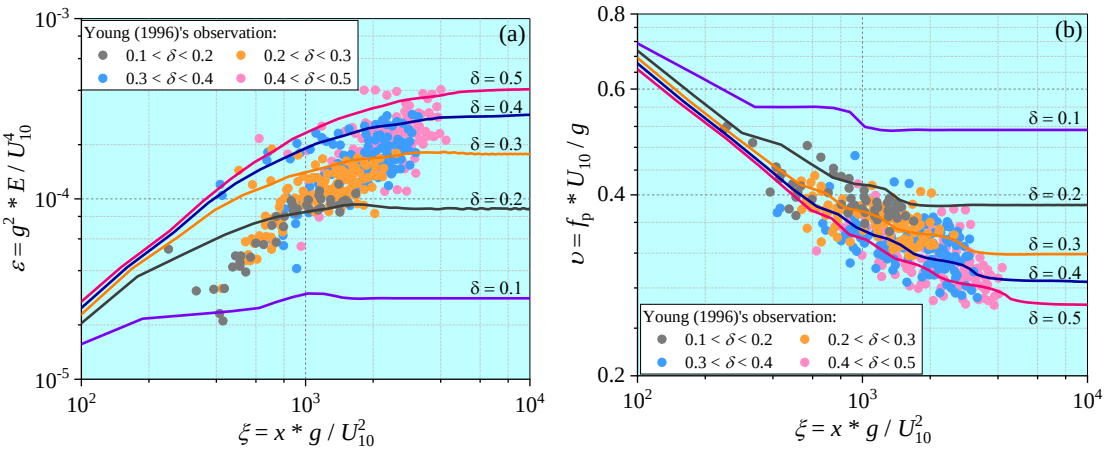

376

377 Figure 5. Comparisons of (a) fetch-limited growth rate and (b) wave age variation between
378 measured and computed results.

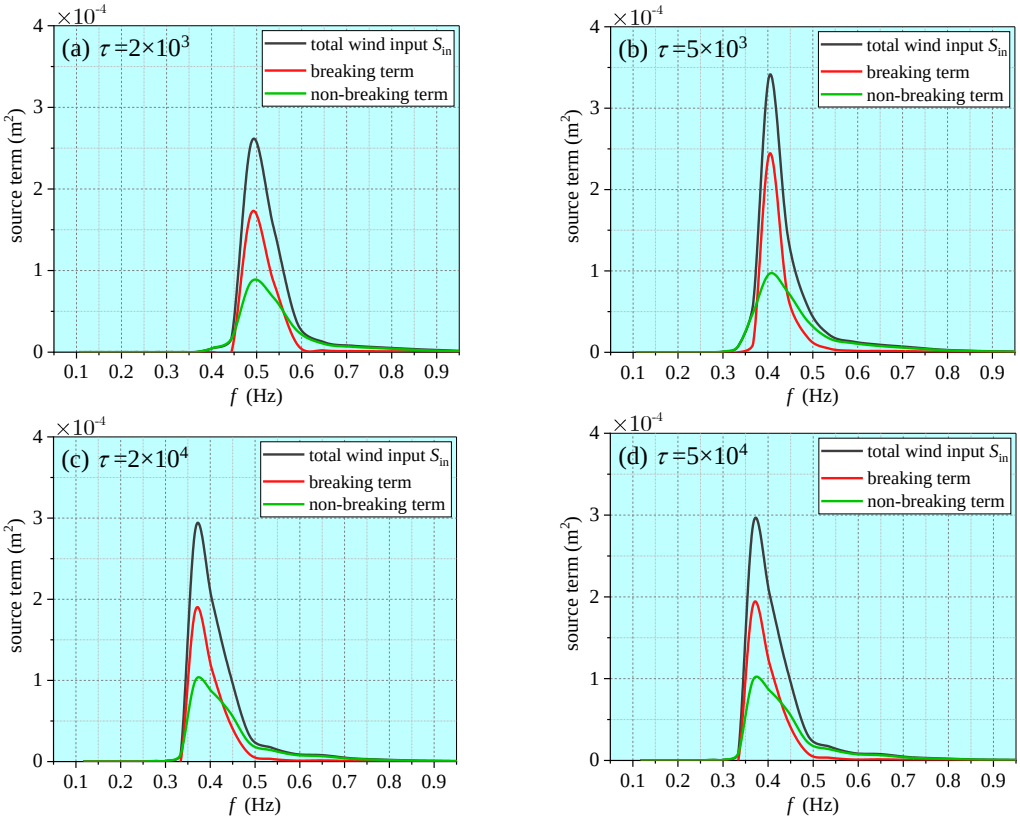

379

380

381 Figure 6. Spectra of wind energy input under breaking and non-breaking conditions resulted
382 from the ST-XY source-term package at different wave development stages in a water depth
383 of 2 m

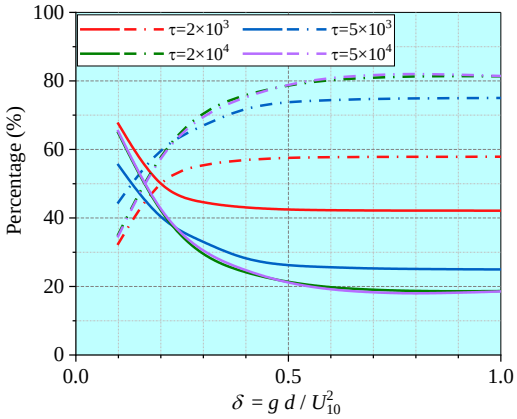

Figure 7. Variations of the percentage for wind energy input under breaking and non-breaking conditions. Solid lines are those under breaking condition while dot-dash lines are those under non-breaking condition. Different colors stand for different wave ages.

Intensified breaking is a major feature of the shallow water waves. Correct representation of the breaking effect in the wind energy input is thus very important for modeling shallow water waves. Different from the deep-water situation, the peak value of the wind energy input taking place under breaking conditions are always higher than under non-breaking conditions all through the early wave-development stage to the equilibrium stage, as presented in Figure 6. The wind energy input taking place under breaking conditions remains a high proportion even at the equilibrium stage, indicating a more frequent breaking in shallow waters. In figure 7, the percentages of the wind energy input taking place under breaking and non-breaking conditions at different water depths and different stage of wave development are shown. At each wave development stage, the percentage taking place under the breaking condition increases as the water depth decreases. At a given water depth, the breaking effect is more prominent at younger wave age but is still important at the equilibrium stage.

4. Model Verification under Practical Extreme Conditions

Storm waves under hurricane winds are characterized by the general young wave age and intensive breaking process, due to the extreme wind speed and rapid-changing wind directions. Therefore, their modeling requires an accurate description of the wind energy input to represent such characteristics. In this section, the effectiveness of the ST-XY

source-term option is evaluated. Hurricane Ivan (2004) and Hurricane Katrina (2005), both of which made landfalls at the coastline of Gulf of Mexico, are chosen for our verification purpose. Hurricanes Ivan and Katrina are both typical, long-lived, category 4-5 tropical cyclones with well recorded observational data. In fact, Hurricanes Ivan and Katrina have been extensively modeled and studied in the literature (Wang et al., 2005; Moon et al., 2008; Fan et al., 2009; Zieger et al., 2015). In addition, since the tracks of the two hurricanes lie in the same ocean basin, data of the topography, the forced wind and the ocean currents can be obtained from the same source, and the model settings can also be kept the same.

4.1 Available data

It is very natural to require possibly most accurate wind data for reliable model results on ocean wave development (Campos et al., 2018). In this study, we blend the H*wind data (resulted from the Real-time Hurricane Wind Analysis System operated by the Hurricane Research Division, National Oceanic and Atmospheric Administration) with the ECMWF (European Centre for Medium-Range Weather Forecasts) data to build the necessary wind field. The H*wind dataset integrates all field data available during a hurricane event and is usually considered to be highly accurate in a certain range affected by the relevant hurricane (Fan et al., 2009; Liu et al., 2017; Chen and Yu, 2017). The H*wind data is issued every 3 h with a grid resolution of 6 km and a spatial extent of 8°×8° around the hurricane center. Because the H*wind data does not cover the entire simulation domain, the ECMWF data must be supplemented. The ECMWF data has a spatial resolution of 0.125° and temporal resolution of 6 h, which is good enough to represent the background wind field. The wind data from different sources is combined by setting a transition zone so that

$$\mathbf{U}_{10}=\begin{cases}\mathbf{U}_{\mathrm{H}} & r<R_{\max}\\ \dfrac{R_{\max}-r}{0.3R_{\max}}\mathbf{U}_{\mathrm{H}}+\dfrac{r-0.7R_{\max}}{0.3R_{\max}}\mathbf{U}_{\mathrm{E}} & 0.7R_{\max}<r<R_{\max}\\ \mathbf{U}_{\mathrm{E}} & r>R_{\max}\end{cases} \tag{13}$$

where, $\mathbf{U}_{\mathrm{H}}$ and $\mathbf{U}_{\mathrm{E}}$ denote the wind velocity vectors from the H*wind dataset and the ECMWF dataset, respectively; r is the distance from the hurricane center; $R_{\max}$ is the

maximal distance of the H*wind boundary to the hurricane center. The time interval of the wind field is interpolated to 0.5 h to satisfy the computational condition. The normalized interpolation method of Fan et al. (2009), which ensures the greatest likelihood that the structure of hurricane wind field is not affected by the interpolation, is applied for this purpose. The wind field constructed in such a manner agrees well with the buoy data as shown in Figures 8 and 9. To include the effect of ocean currents (Fan et al., 2009), the global reanalysis database generated with HYCOM (HYbrid Coordinate Ocean Model) and NCODA (Navy Coupled Ocean Data Assimilation) is also utilized as the model input. The data has a spatial resolution of 1/12° and a temporal resolution of 3 h. The topography data is from the ETOPO1 datasets and has a spatial resolution of 1'.

Buoy data published by NDBC (National Data Buoy Center, National Oceanic and Atmospheric Administration) are used to validate the model results on representative wave parameters including H_s, T_{02} and spectral wave parameters in both deep- and shallow waters. The locations of buoys are shown in Figure 10.

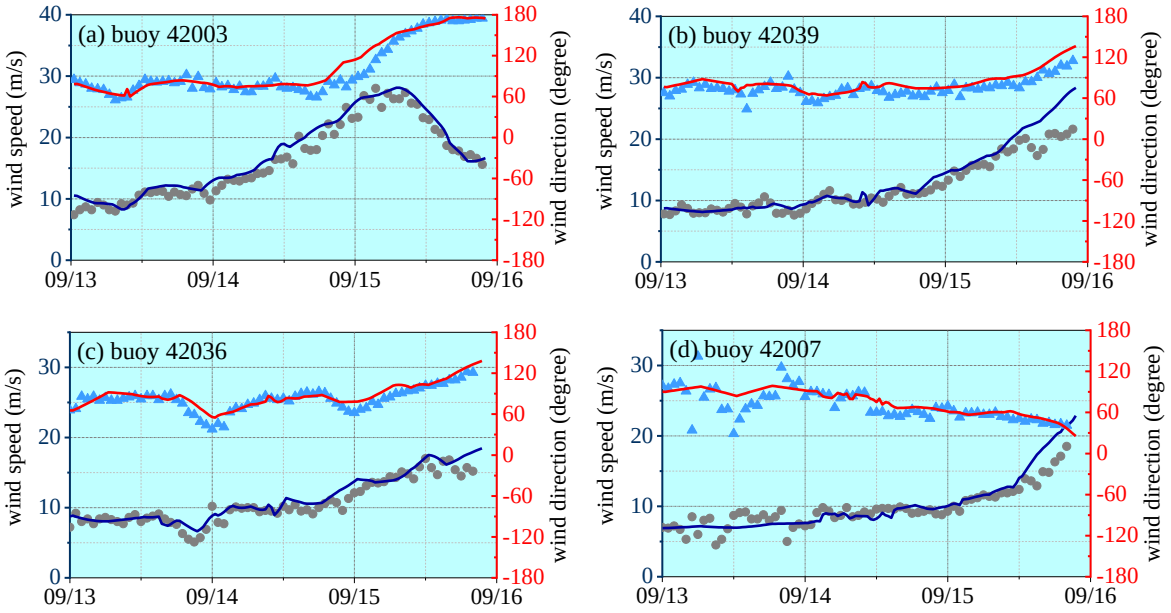

Figure 8. Comparison of reconstructed time series of wind velocity with observed data at locations of the NDBC buoys during Hurricane Ivan. Scattered dots and triangles are buoy data of wind speed and wind direction, respectively. Blue and red lines are constructed wind speed and wind direction, respectively.

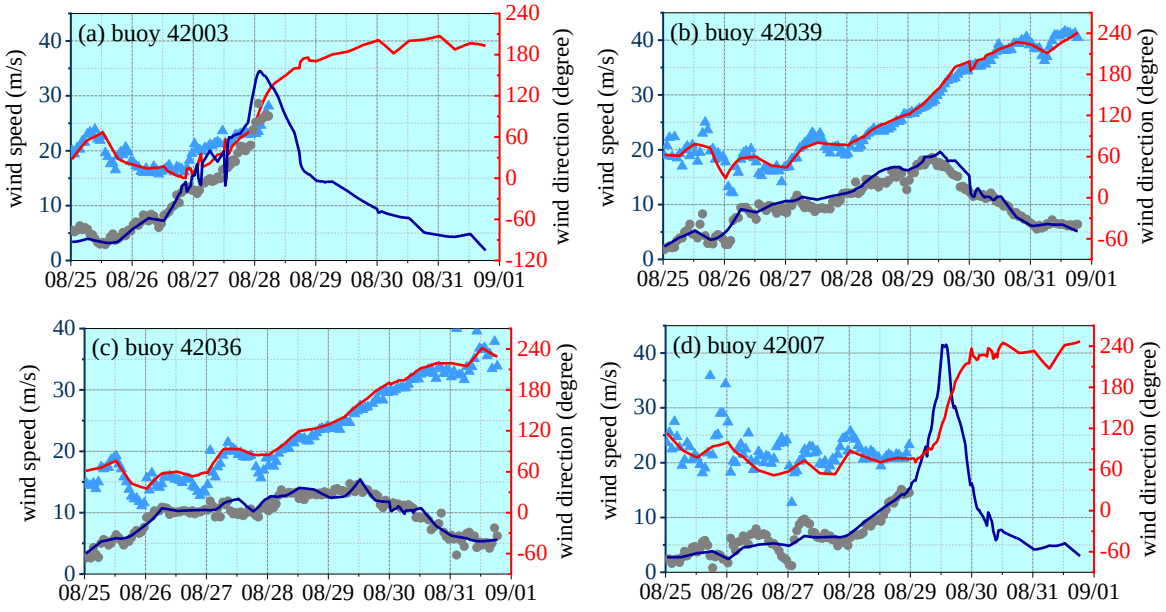

Figure 9. Comparison of reconstructed time series of wind velocity with observed data at locations of the NDBC buoys during Hurricane Katrina. Scattered dots and triangles are buoy data of wind speed and wind direction, respectively. Blue and red lines are constructed wind speed and wind direction, respectively. At buoy 42003 and 42007, there is data missing.

4.2 Model setup

The computational domain, as shown in Figure 10, covers the area affected by both Hurricane Ivan (2004) and Hurricane Katrina (2005), ranging from 100°W to 82°W and from 18°N to 32°N within Gulf of Mexico. Considering a minimal time period for model warm-up, simulation of Hurricane Ivan is initialized at 00:00 UTC, 12 September 2004 and continues for nearly 4 days until 21:00 UTC, 15 September 2004. Simulation of Hurricane Katrina is initialized at 00:00 UTC, 25 August 2005 and continues for nearly 7 days until 18:00 UTC, 31 August 2005. A time step of 10 min is fixed. The simulation is performed over the geographical coordinate system with a resolution of 1/12°. We assume 36 directional intervals with a constant increment of 10° and 35 frequency intervals that increase logarithmically over the range of 0.0373-1.048 Hz. The numerical results obtained with the ST-XY source-term option are compared to those obtained with other options. The ST2, ST4, ST6 options are implemented with the default setting.

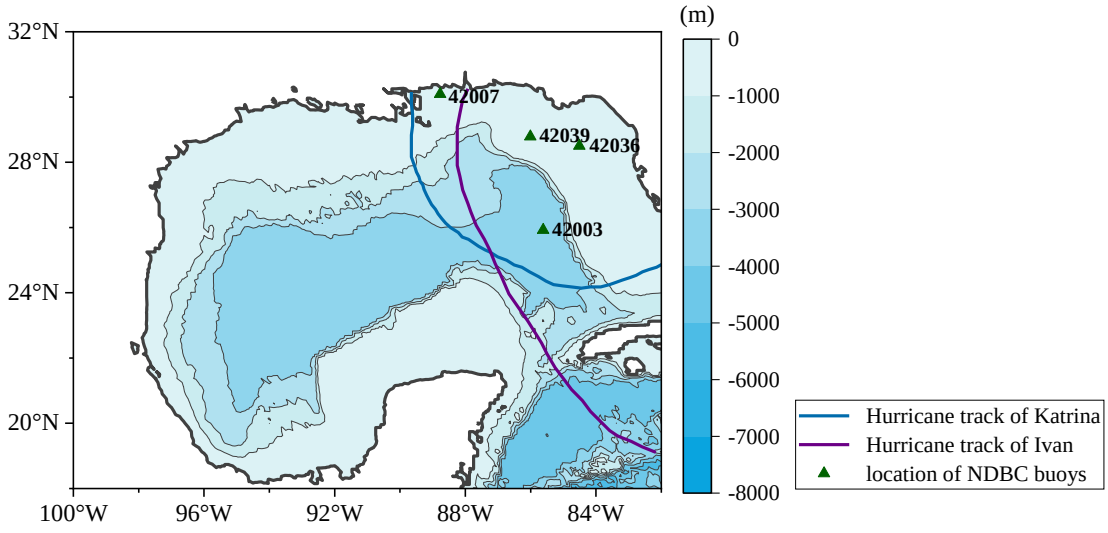

Figure 10. The computational domain. Tracks of hurricanes are shown with solid lines. The NDBC buoys are marked by triangles. Water depth at the locations of buoys 42003, 42039, 42036 and 42007 are 3265 m, 281 m, 50.9 m and 14.9 m, respectively.

4.3 Comparison of wave parameters

The model results on the time variations of the significant wave height H_s and the mean wave period T_{02} at the locations of the buoys during Hurricane Ivan and Hurricane Katrina are shown in Figures 11 and 12, respectively. The observed data are also plotted for comparison. It can be seen that the significant wave height H_s obtained with the ST-XY option agrees fairly well with the buoy data and performs better than the ST2 and ST6 options. The peak value and peak time of the significant wave height are accurately represented. In comparison, the significant wave height H_s is obviously overestimated by the ST6 option but underestimated by the ST2 option. The ST4 option performs also very well, but still show some underestimation of the peak values of H_s (as shown in Figures 11a and 12a) and some overestimation of H_s before it reaches its maximum value (as shown in Figures 11b-d). The numerical results for the mean wave period T_{02} are shown to be generally less accurate than those for the significant wave height H_s, especially during the period before and after the hurricane event. A possible reason is that the total wave energy is paid more attention when formulating source terms of the wave model while the statistical laws for wave period are usually less accurate under relatively calm sea conditions. Note that an underestimation of T_{02} is evident, but the peak values of T_{02} are still reasonably

simulated. The mean absolute error (MAE) and root mean square error (RMSE) for each hurricane event are shown in Tables 1 and 2. It is demonstrated that the ST-XY has outstanding performance on H_s with obviously smaller MAE and RMSE values. The performance of ST4 is also satisfactory as compared to ST2 and ST6.

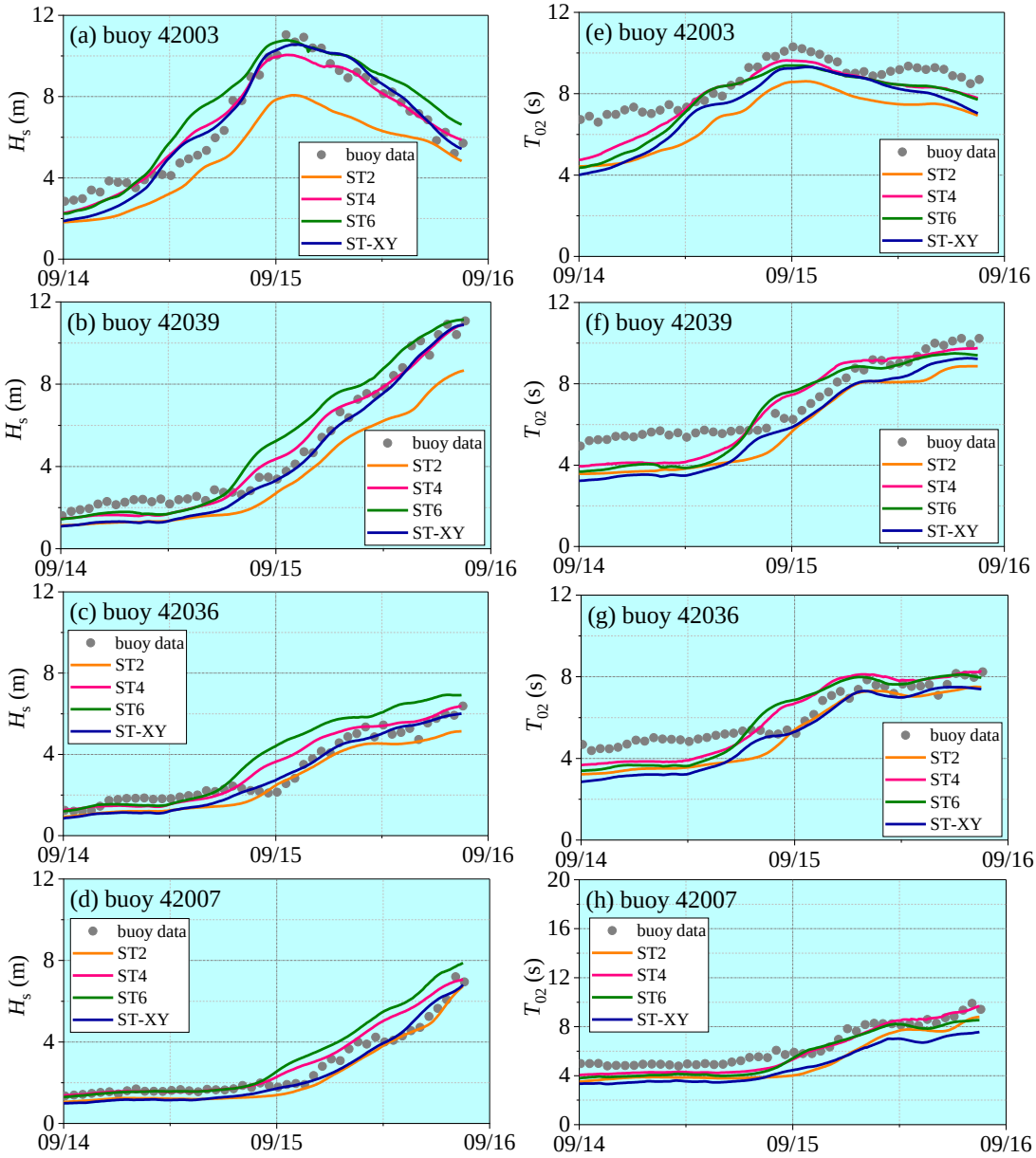

Figure 11. Comparisons of the computed variations (lines) of (a) – (d) H_s and (e) – (h) T_{02} with buoy data (dots) during Hurricane Ivan.

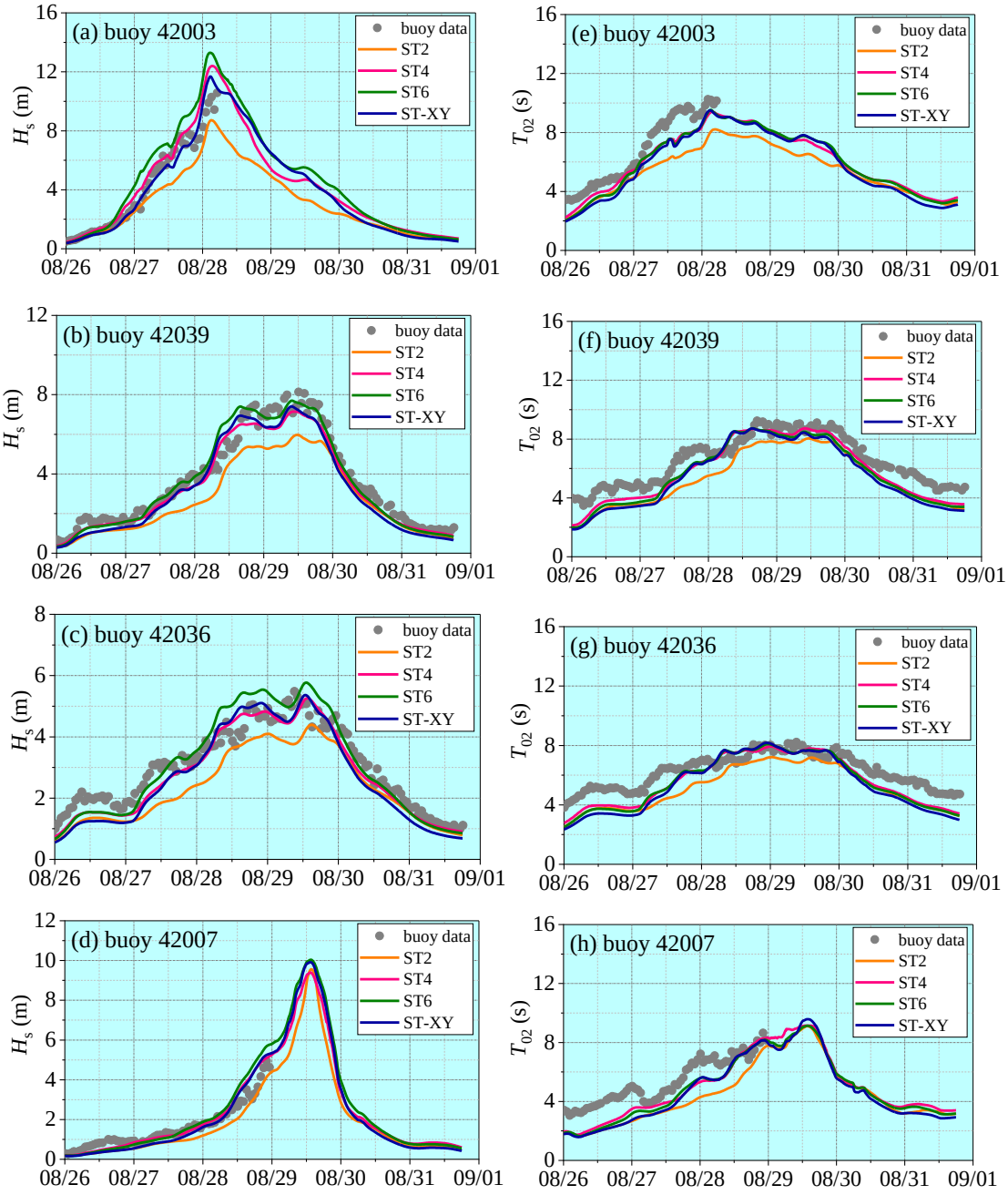

Figure 12. Comparisons of the computed variations (lines) of (a) – (d) H_s and (e) – (h) T_{02} with buoy data (dots) during Hurricane Katrina.

509 Table 1. Simulation errors in wave parameters during Hurricane Ivan.

		ST2		ST4		ST6		ST-XY	
		MAE	RMSE	MAE	RMSE	MAE	RMSE	MAE	RMSE
42003	H_s (m)	1.96	2.10	0.36	0.48	0.72	0.83	0.33	0.41
	T_{02} (s)	1.53	1.54	0.56	0.62	0.65	0.69	0.86	0.94
42039	H_s (m)	1.52	1.67	0.53	0.62	1.08	1.20	0.33	0.40
	T_{02} (s)	1.01	1.06	0.54	0.63	0.58	0.70	0.69	0.72
42007	H_s (m)	0.45	0.52	0.61	0.72	1.01	1.13	0.37	0.44
	T_{02} (s)	1.27	1.37	0.44	0.54	0.54	0.68	1.54	1.58
42036	H_s (m)	0.51	0.58	0.62	0.75	1.34	1.42	0.26	0.32
	T_{02} (s)	0.44	0.52	0.61	0.72	0.60	0.78	0.37	0.43

510

511 Table 2. Simulation errors in wave parameters during Hurricane Katrina.

		ST2		ST4		ST6		ST-XY	
		MAE	RMSE	MAE	RMSE	MAE	RMSE	MAE	RMSE
42003	H_s (m)	1.40	1.56	1.00	1.28	1.83	2.03	0.71	0.88
	T_{02} (s)	2.20	2.32	1.09	1.21	1.11	1.23	1.26	1.38
42039	H_s (m)	0.99	1.17	0.41	0.52	0.37	0.53	0.54	0.62
	T_{02} (s)	1.19	1.26	0.71	0.80	0.82	0.90	1.00	1.10
42007	H_s (m)	0.47	0.51	0.25	0.40	0.39	0.60	0.35	0.45
	T_{02} (s)	1.68	1.80	0.87	1.01	0.88	1.00	1.02	1.16
42036	H_s (m)	0.67	0.78	0.32	0.39	0.40	0.51	0.45	0.52
	T_{02} (s)	1.06	1.16	0.72	0.82	0.76	0.87	0.91	1.06

512

513 **4.4 Comparison of wave spectra**

514 For the detailed description of a wave spectrum, the peak value E_p, the peak
515 frequency f_p of the spectrum as well as its mean square slope M_s are defined to describe
516 the frequency spectrum; the dominant wave propagation direction θ_m, the mean wave
517 propagation direction $\bar{\theta}$ and the directional spreading width $\Delta\theta$ are defined to describe
518 the directional spectrum. In particular,

519 $$E_p = \max\left(\int_0^{2\pi} E\ f,\theta\ d\theta\right) \tag{14}$$

520 $$M_s = \iint k^2 E\ f,\theta\ dfd\theta \tag{15}$$

$$E\ \theta_{\mathrm{m}}\ = \max\ \int E\ f,\theta\ df \tag{16}$$

$$E\ \theta_{\mathrm{e}}\ \geq 0.1\max\ \int E\ f,\theta\ df \tag{17}$$

$$\overline{\theta} = \frac{1}{2}\ \theta_{\mathrm{e1}} + \theta_{\mathrm{e2}} \tag{18}$$

$$\Delta\theta = \theta_{\mathrm{e2}} - \theta_{\mathrm{e1}} \tag{19}$$

where, E_{p} is the peak value of the frequency spectrum, f_{p} is the corresponding peak frequency; M_{s} is the mean square slope of frequency spectrum, representing the effect of high-frequency wave components; $E\ \theta_{\mathrm{m}}$ is the peak of the directional spectrum and θ_{m} is the corresponding direction, called the main wave direction; θ_{e} is called the efficient wave direction beyond which the wave energy is below 10% of the peak value of the directional spectrum; θ_{e1} and θ_{e2} are the lower and higher limits of θ_{e}; $\overline{\theta}$ is the mean wave propagation direction while $\Delta\theta$ is the directional range of the effective wave propagation.

Comparison of the computed wave spectra with observations is made at the locations of buoys 42039 and 42036, where a relatively complete data series have been recorded during both hurricane events. Variations of the spectral wave parameters in the deep-water condition (at buoy 42039) are presented in Figures 13 and 14 while those in the shallow water condition (at buoy 42036) are presented in Figures 15 and 16. Accuracy of the numerical results for the peak spectrum value E_{p} is quite similar to that for the representative wave parameters such as H_{s}. The result obtained with the ST-XY option can catch the extreme wave energy condition very well, while the ST6 option always overestimate and the ST2 option underestimate it. The result obtained with the ST4 option overestimates E_{p} under the moderate wind conditions before the extreme events. The numerical results for the peak frequency f_{p} agrees with observations well during both hurricane events. M_{s} is also satisfactorily simulated, which means that the high frequency part of the wave spectrum is well described by the numerical model. It may be necessary to point out that, different from the results for the representative wave parameters, the peak of

547 E_p may not be correctly represented by any package of the source terms under our
548 consideration in some cases, as shown in Figure 14a.

549
550
551
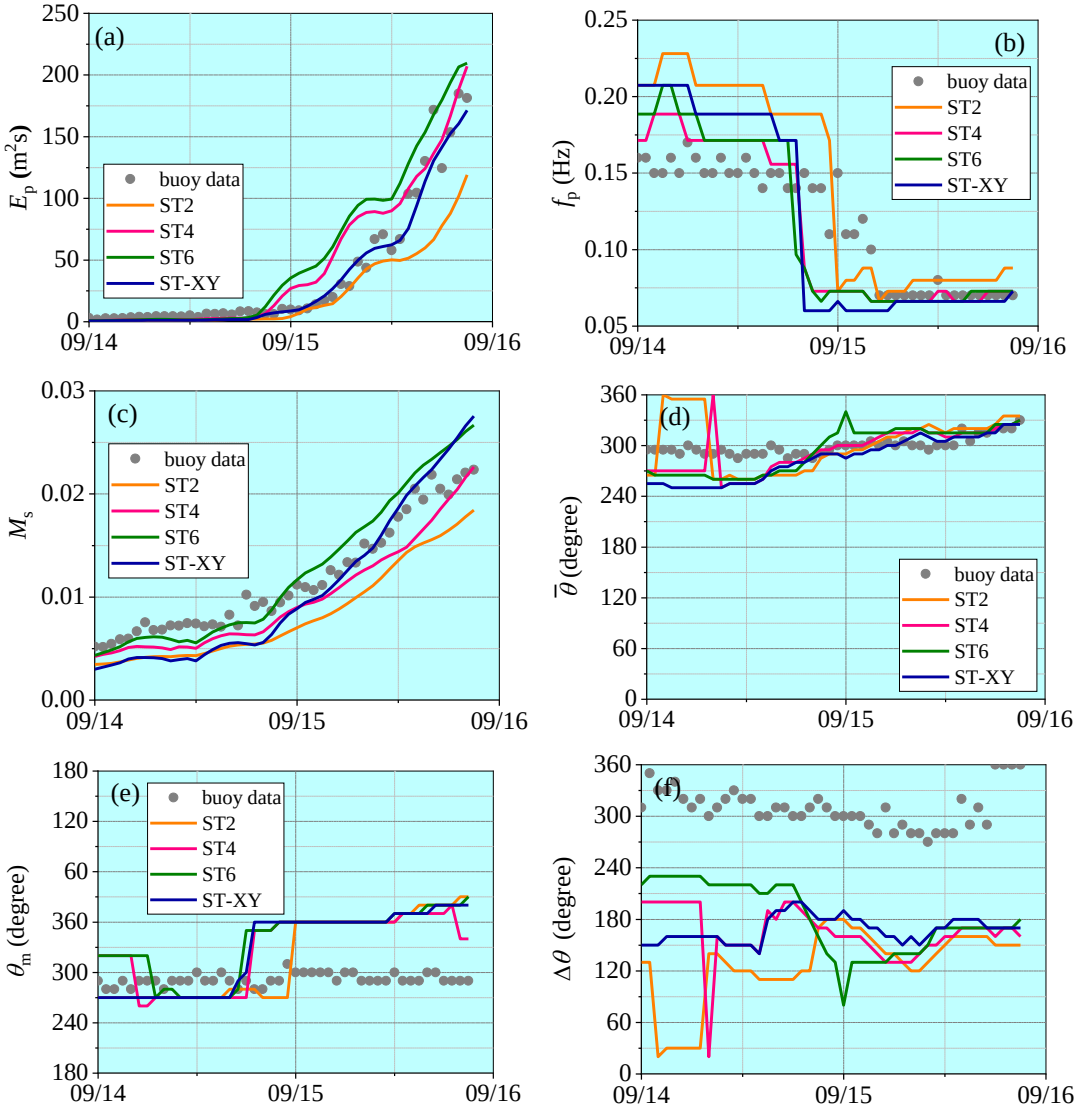

552 Figure 13. Comparisons of wave spectral parameters with observations at buoy 42039
553 during Hurricane Ivan. (a) spectrum peak value; (b) peak frequency; (c) mean square slope;
554 (d) mean wave propagation direction; (e) main wave propagation direction; (f) wave
555 propagation spread width.

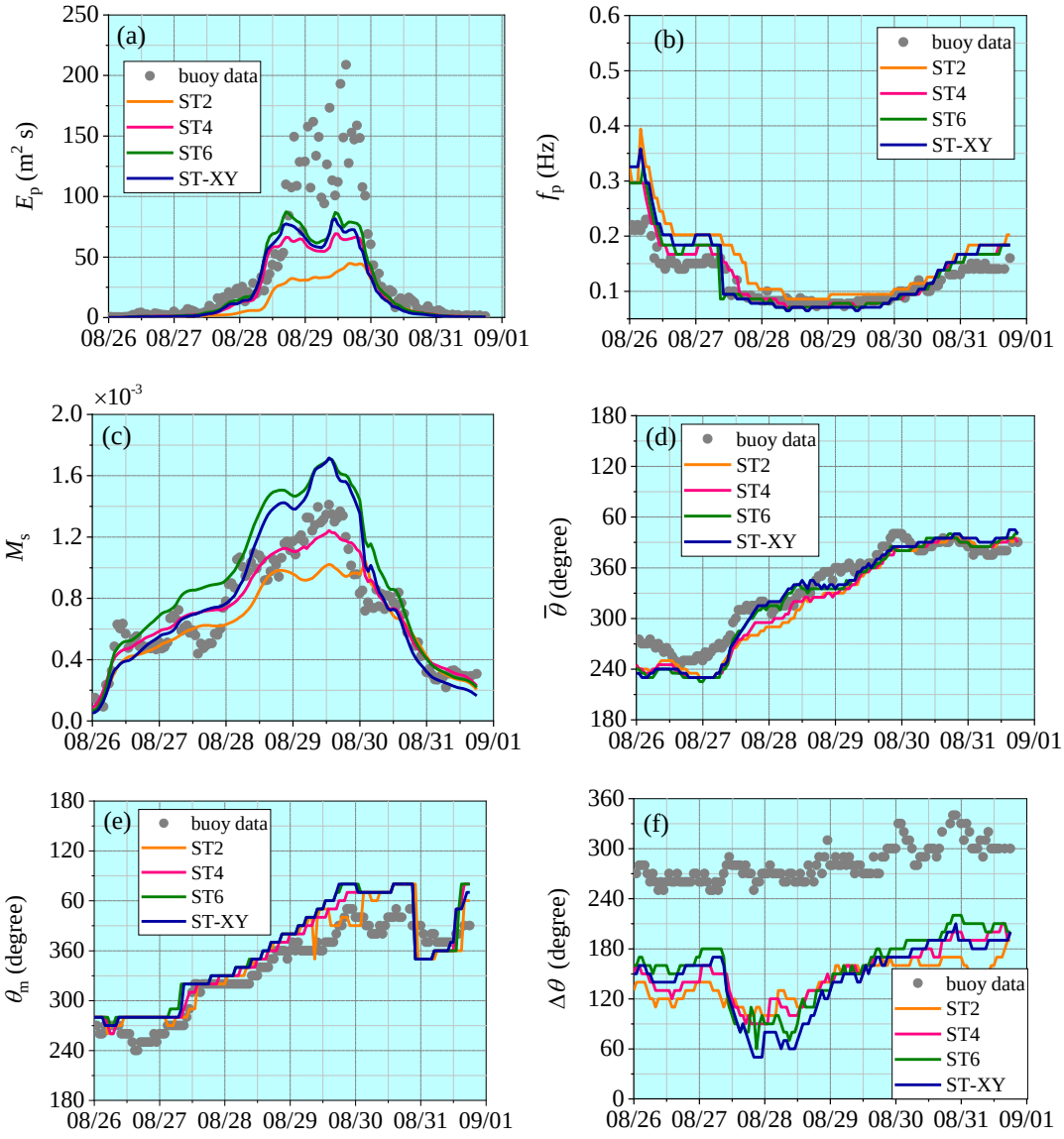

Figure 14. Comparisons of wave spectral parameters with observations at buoy 42039 during Hurricane Katrina. (a) spectrum peak value; (b) peak frequency; (c) mean square slope; (d) mean wave propagation direction; (e) main wave propagation direction; (f) wave propagation spread width.

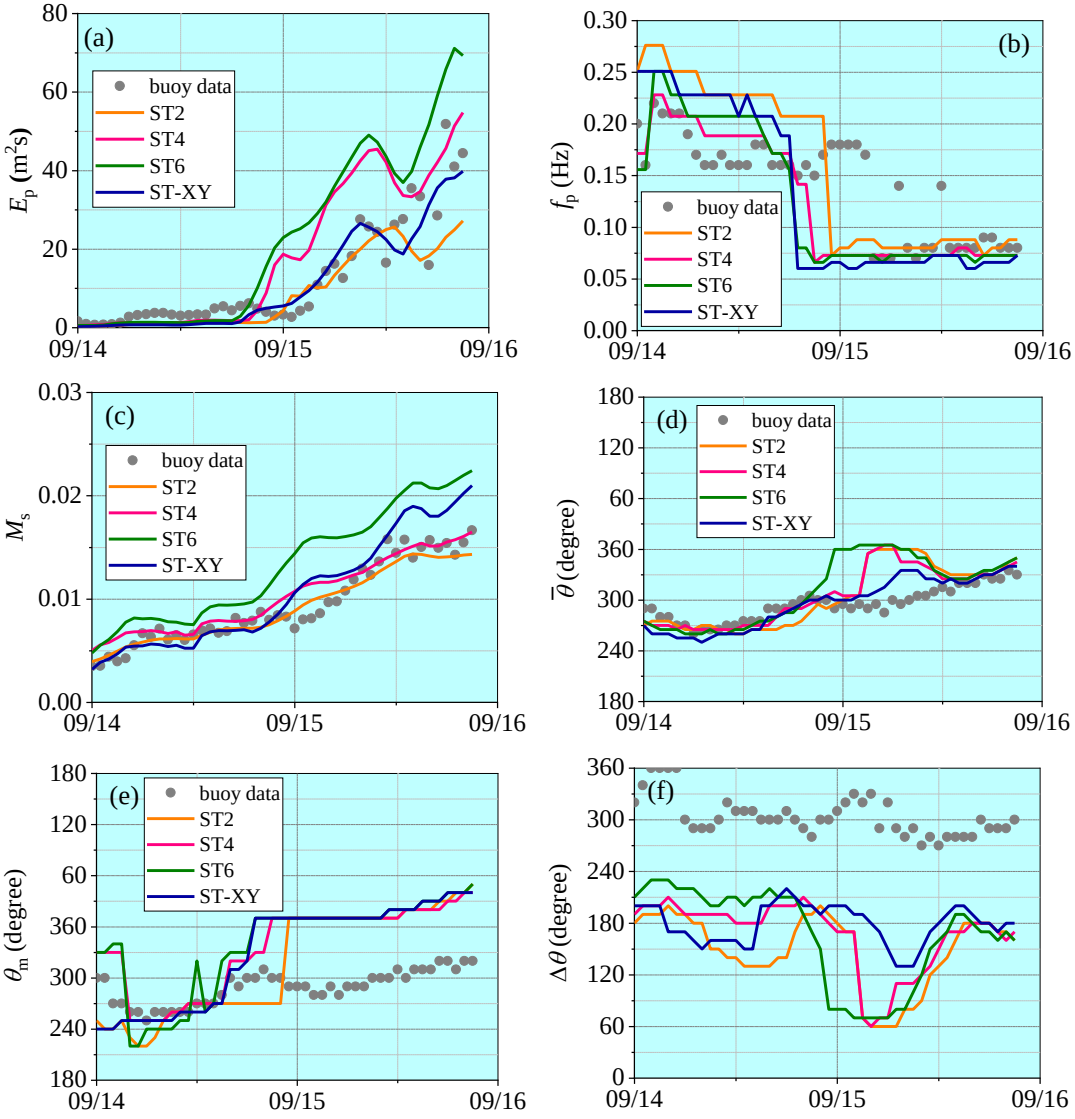

Figure 15. Comparisons of wave spectral parameters with observations at buoy 42036 during Hurricane Ivan. (a) spectrum peak value; (b) peak frequency; (c) mean square slope; (d) mean wave propagation direction; (e) main wave propagation direction; (f) wave propagation spread width.

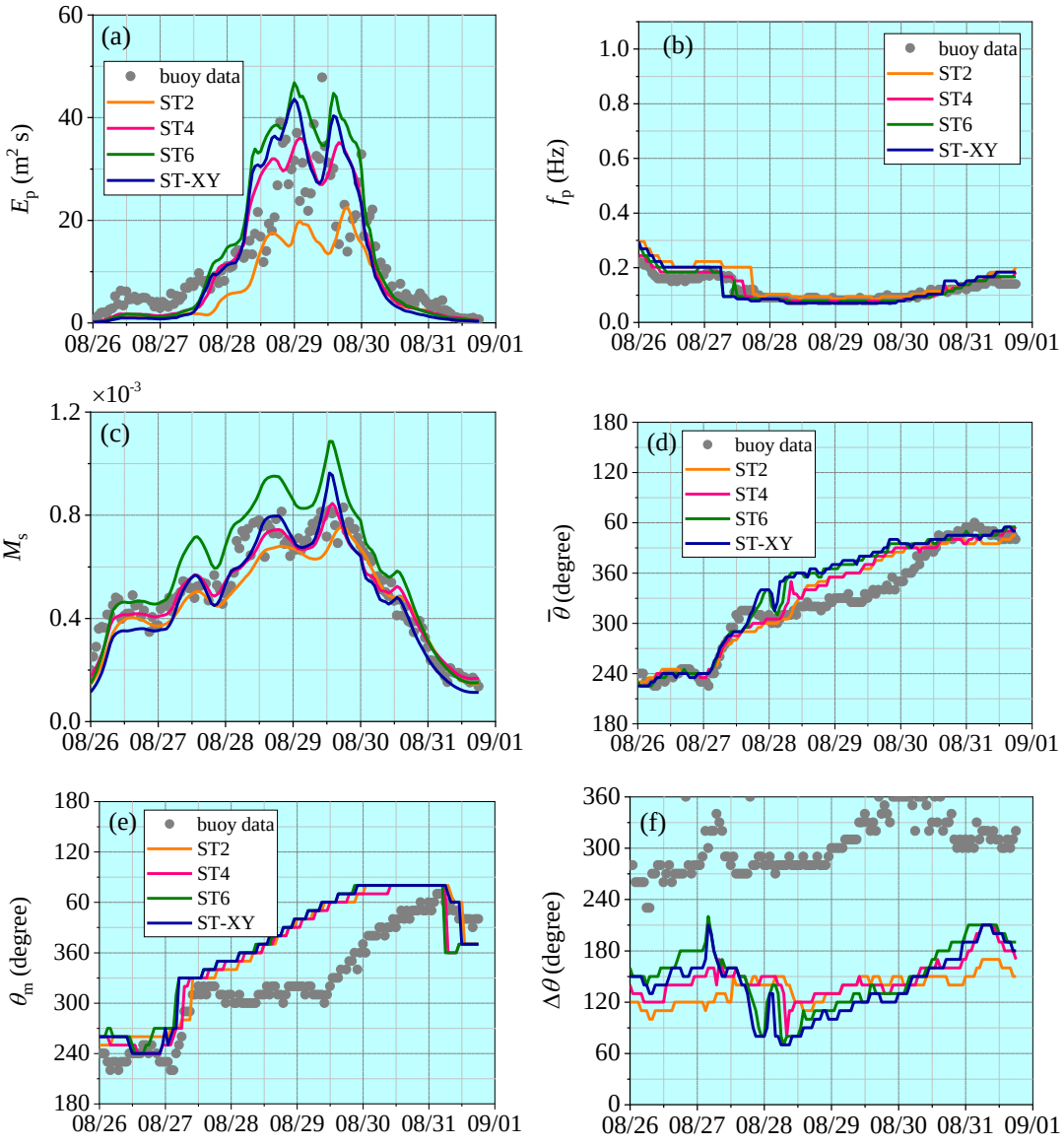

Figure 16. Comparisons of wave spectral parameters with observations at buoy 42036 during Hurricane Katrina. (a) spectrum peak value; (b) peak frequency; (c) mean square slope; (d) mean wave propagation direction; (e) main wave propagation direction; (f) wave propagation spread width.

It is also demonstrated that the numerical results for the main wave propagation direction and the mean wave propagation direction obtained with the ST-XY option and other source-term options are all equally good. However, the numerical result for the directional range of the effective wave propagation is obvious narrower than observed one. This, however, may not be an error of the numerical model since the directional range of the effective wave propagation depends significantly on the methods employed (Earle et al.,

1999; Kim et al., 1995). In this study, Longuet-Higgins' method (Longuet-Higgins et al., 1963) is used to build the directional wave spectrum from observed data. This method always leads a broader directional spectrum than other methods with the same parameters (Earle et al. (1999)'s Figure 2).

Waves under hurricane condition break more frequently and severely than under normal condition due to high wind speed and rapidly transforming wind direction, leading to a relatively large amount of wind energy input into the breaking wave components and also an increased total wind energy input. On the other hand, severe wave breaking under hurricane condition also causes high wave energy dissipation. Therefore, a careful consideration of the effect of wave breaking is very important for simulation of wave development under the action of tropical cyclones. Since evolution of the wave spectrum depends on the net effect of the wind energy input and the wave energy dissipation, while it is difficult to identify a decrease of wind energy input from an increase of wave energy dissipation, particularly under extreme sea state, we emphasize that the wind energy input proposed by Xu and Yu (2020) and the wave energy dissipation extended from that of Ardhuin et al. (2010) must be considered as a set.

5. Conclusion

This study is aimed to evaluate the performance of the improved formulas for the wind energy input and the wave energy dissipation, i.e., the ST-XY source-term option. The numerical results are obtained with the coupled AWBLM-WWIII model. Both duration-limited waves under idealized conditions and hurricane-generated waves, in both deep and shallow waters are studied. The standard source-term packages of ST2, ST4 and ST6 embedded in WWIII are chosen for comparison. Detailed comparisons are made for not only the representative wave parameters, including the significant wave height, the mean wavelength and the mean wave period, but also the characteristic parameters for the frequency spectrum and the directional spreading function. The effect of breaking on ocean wave modeling is fully discussed.

The numerical results show that the ST-XY source-term package performs better than

611 other standard options in general. At the early wave-development stage, the ST-XY option
612 leads to a better agreement of the computed wave energy with the empirical results while
613 other source-term options all tend to underestimate the wave energy. At the equilibrium
614 stage, the results obtained with the ST-XY option approaches the Pierson-Moskowitz limit
615 while ST2 option significantly underestimates the wave energy. The ST-XY option is also
616 effective for ocean wave modeling under both deep- and shallow- water conditions and
617 gives results in good agreement with field data. For hurricane-generated waves, model
618 results obtained with the ST-XY option agrees well with the buoy data and are obviously
619 better than those obtained with other source-term options. On the other hand, the ST6 option
620 often overestimates wave energy while ST2 option leads to an obvious underestimation. The
621 ST4 option performs fairly well but still show some underestimation of the peak value of
622 significant wave height and some overestimation of the significant wave height before its
623 peak value is achieved.

624 Wave breaking significantly affect ocean wave modeling, especially at younger wave
625 ages and in shallower waters. At the early wave-development stage, a significant part of the
626 peak wind energy input takes place under breaking condition, and the proportion decreases
627 gradually as the wave development continues. In shallow waters, the peak value of wind
628 energy input taking place under breaking conditions are always higher than that under
629 non-breaking conditions throughout the early wave-development stage to the equilibrium
630 stage.

631 In summary, the improved formula of Xu and Yu (2020), which includes both breaking
632 effect and the effect of air-flow separation on the leesides of steep wave crests in a
633 consistent way, has a satisfactory performance within the coupled AWBLM-WWIII model.
634 It is physics-based and is verified to be effective for ocean wave modeling under both
635 moderate and extreme wind conditions, at all wave-development stages, and in deep to
636 shallow waters, thus has a broad applicability.

637 ## Competing interests

638 The authors declare that there is no conflict of interest.

Authors' contributions

Y. Xu and X. Yu conceived of the presented idea. Y. Xu performed the computations. X. Yu supervised the project. Both authors discussed the results and contributed to the final manuscript.

Funding

This research is supported by National Natural Science Foundation of China (NSFC) under grant No. 11732008.

Code Availability

The code used in this work can be found at https://doi.org/10.5281/zenodo.7047221 (Xu and Yu, 2022a). The input files of the controlled normal-condition cases can be found at https://doi.org/10.5281/zenodo.7047234 (Xu and Yu, 2022b). The input files of hurricane Ivan case can be found at https://doi.org/10.5281/zenodo.7047240 (Xu and Yu, 2022c). The input files of hurricane Katrina case can be found at https://doi.org/10.5281/zenodo.7047244 (Xu and Yu, 2022d).

Data Availability

The H*wind data are available at https://www.rms.com/event-response/hwind. The ECMWF-ERA5 wind data are available upon request to https://www.ecmwf.int/. The topography data are available at https://www.ngdc.noaa.gov/mgg/global/global.html. The buoy data can be obtained from NOAA at https://www.ndbc.noaa.gov/.

References

Ardhuin, F., Rogers, E., Babanin, A. V., Filipot, J. F., Magne, R., Roland, A., et al. (2010). Semiempirical dissipation source functions for ocean waves. Part I. definition, calibration, and validation. Journal of Physical Oceanography, 40(9): 1917-1941.

Babanin, A. V. and Young, I. R. (2005). Two-phase behaviour of the spectral dissipation of wind waves. Proceedings of the 5th International Symposium on Ocean Waves

664 Measurement and Analysis, Madrid, Spain, Paper No. 51.
665 Babanin, A. V., Banner, M. L., Young, I. R., and Donelan, M. A. (2007). Wave-follower
666 field measurements of the wind-input spectral function. Part III: Parameterization of
667 the wind-input enhancement due to wave breaking. Journal of Physical Oceanography,
668 37(11), 2764-2775.
669 Badulin, S. I., Babanin, A. V., Zakharov, V. E., and Resio, D. (2007). Weakly turbulent laws
670 of wind-wave growth. Journal of Fluid Mechanics, 591: 339-378.
671 Banner, M. L., and Melville, W. K. (1976). On the separation of air flow over water waves.
672 Journal of fluid mechanics, 77(4), 825-842.
673 Battjes, J. A., and Janssen, J. P. F. M. (1978). Energy loss and set-up due to breaking of
674 random waves. In Coastal engineering 1978 (pp. 569-587).
675 Beyá, J., Álvarez, M., Gallardo, A., Hidalgo, H., and Winckler, P. (2017). Generation and
676 validation of the Chilean Wave Atlas database. Ocean Modelling, 116, 16-32.
677 Campos, R. M., Alves, J. H. G. M., Soares, C. G., Guimaraes, L. G., and Parente, C. E.
678 (2018). Extreme wind-wave modeling and analysis in the south Atlantic ocean. Ocean
679 Modelling, 124, 75-93.
680 Cavaleri, L., Alves, J. H., Ardhuin, F., Babanin, A., Banner, M., Belibassakis, K., ... and
681 WISE Group. (2007). Wave modelling–the state of the art. Progress in oceanography,
682 75(4), 603-674.
683 Cavaleri, L., Barbariol, F., and Benetazzo, A. (2020). Wind–wave modeling: Where we are,
684 where to Go. Journal of Marine Science and Engineering, 8(4), 260.
685 CERC (1977). Shore protection manual. U.S. Army Coastal Research Center, Vols. 1–3.
686 Chalikov, D. (1995). The parameterization of the wave boundary layer. Journal of Physical
687 Oceanography, 25(6), 1333-1349.
688 Chalikov, D. V., and Belevich, M. Y. (1993). One-dimensional theory of the wave boundary
689 layer. Boundary-Layer Meteorology, 63(1-2), 65-96.
690 Chen, Y. and Yu, X. (2017). Sensitivity of storm wave modeling to wind stress evaluation
691 methods. Journal of Advances in Modelling Earth System, 9: 893-907.
692 Csanady, G. T. (2001). Air-Sea Interaction: Laws and Mechanisms. Cambridge University

693 Press, New York.
694 Donelan, M. A., and Pierson Jr, W. J. (1987). Radar scattering and equilibrium ranges in
695 wind-generated waves with application to scatterometry. Journal of Geophysical
696 Research: Oceans, 92(C5): 4971-5029.
697 Donelan, M. A., Babanin, A. V., Young, I. R., and Banner, M. L. (2006). Wave-follower
698 field measurements of the wind-input spectral function. Part II: Parameterization of the
699 wind input. Journal of physical oceanography, 36(8): 1672-1689.
700 Donelan, M.A., (2001). A nonlinear dissipation function due to wave breaking. Proceedings
701 of ECMWF Workshop on Ocean Wave Forecasting, 87–94, ECMWF, Reading, U.K.
702 Earle, M. D., Steele, K. E., and Wang, D. W. C. (1999). Use of advanced directional wave
703 spectra analysis methods. Ocean engineering, 26(12), 1421-1434.
704 Eldeberky, Y. (1996). Nonlinear transformationations of wave spectra in the nearshore zone.
705 Unpublished doctoral dissertation, Delft University of Technology, Delft, The
706 Netherlands.
707 Fan, Y., and Rogers, W. E. (2016). Drag coefficient comparisons between observed and
708 model simulated directional wave spectra under hurricane conditions. Ocean Modelling,
709 102, 1-13.
710 Fan, Y., Ginis, I., Hara, T., Wright, C. W., and Walsh, E. J. (2009). Numerical simulations
711 and observations of surface wave fields under an extreme tropical cyclone. Journal of
712 Physical Oceanography, 39(9), 2097-2116.
713 Hasselmann, K. (1974). On the spectral dissipation of ocean waves due to white capping.
714 Boundary-Layer Meteorology, 6(1-2): 107-127.
715 Hasselmann, K., Barnett, T. P., Bouws, E., Carlson, H., Cartwright, D. E., Enke, K. et al.
716 (1973). Measurements of wind-wave growth and swell decay during the Joint North
717 Sea Wave Project (JONSWAP). Ergänzungsheft, 8-12.
718 Hwang, P. A. (2005). Temporal and spatial variation of the drag coefficient of a developing
719 sea under steady wind-forcing. Journal of Geophysical Research: Oceans, 110(C7).
720 Hwang, P. A., and Wang, D. W. (2004). An empirical investigation of source term balance of
721 small scale surface waves. Geophysical research letters, 31(15).

Janssen, P. A. E. M. (1989). Wave-induced stress and the drag of air flow over sea waves. Journal of Physical Oceanography, 19(6): 745-772.

Janssen, P. A. E. M. (1991). Quasi-linear theory of wind-wave generation applied to wave forecasting. Journal of Physical Oceanography, 21(21): 1631-1642.

Janssen, P. A. E. M. (2004), The Interaction of Ocean Waves and Wind. Cambridge University Press, Cambridge, U.K.

Jones, I. S. and Toba, Y. (2001). Wind Stress over the Ocean. Cambridge University Press, New York.

Kahma, K. K., and Calkoen, C. J. (1992). Reconciling discrepancies in the observed growth of wind-generated waves. Journal of Physical Oceanography, 22(12), 1389-1405.

Kim, T., Lin, L. H., and Wang, H. (1995). Application of maximum entropy method to the real sea data. In Coastal Engineering 1994 (pp. 340-355).

Leckler, F., Ardhuin, F., Filipot, J. F., and Mironov, A. (2013). Dissipation source terms and whitecap statistics. Ocean Modelling, 70: 62-74.

Liu, Q., Babanin, A., Fan, Y., Zieger, S., Guan, C., and Moon, I. J. (2017). Numerical simulations of ocean surface waves under hurricane conditions: Assessment of existing model performance. Ocean Modelling, 118, 73-93.

Longuet-Higgins, M. S. (1969). On wave breaking and the equilibrium spectrum of wind-generated waves. Proceedings of the Royal Society of London. A. Mathematical and Physical Sciences, 310(1501), 151-159.

Longuet-Higgins, M. S., Cartwright, D. E., and Smith, N. D. (1963). "Observations of the Directional Spectrum of Sea Waves Using The Motion of a Floating Buoy", in Ocean Wave Spectra, Prentice Hall, Englewood Cliffs, N. J., pp.111-136.

Makin, V. K., and Kudryavtsev, V. N. (1999). Coupled sea surface-atmosphere model: 1. Wind over waves coupling. Journal of Geophysical Research: Oceans, 104(C4), 7613-7623.

Melville, W. K. and Matusov, P. (2002). Distribution of breaking waves at the ocean surface. Nature, 417: 58.

Mentaschi, L., Besio, G., Cassola, F., and Mazzino, A. (2015). Performance evaluation of

751 Wavewatch III in the Mediterranean Sea. Ocean Modelling, 90, 82-94.
752 Miles, J. W. (1957). On the generation of surface waves by shear flows. Journal of Fluid
753 Mechanics, 3(2): 185-204.
754 Miles, J. W. (1965). A note on the interaction between surface waves and wind profiles.
755 Journal of Fluid Mechanics, 22(4): 823-827.
756 Moon, I. J., Ginis, I., and Hara, T. (2008). Impact of the reduced drag coefficient on ocean
757 wave modeling under hurricane conditions. Monthly Weather Review, 136(3),
758 1217-1223.
759 Moskowitz, L. (1964). Estimates of the power spectrums for fully developed seas for wind
760 speeds of 20 to 40 knots. Journal of geophysical research, 69(24), 5161-5179.
761 Phillips, O. M. (1985). Spectral and statistical properties of the equilibrium range in
762 wind-generated gravity waves. Journal of Fluid Mechanics, 156: 505-531.
763 Phillips, O. M., Posner, F. L., and Hansen, J. P. (2001). High range resolution radar
764 measurements of the speed distribution of breaking events in wind-generated ocean
765 waves: surface impulse and wave energy dissipation rates. Journal of Physical
766 Oceanography, 31: 450-460.
767 Pierson Jr, W. J., and Moskowitz, L. (1964). A proposed spectral form for fully developed
768 wind seas based on the similarity theory of SA Kitaigorodskii. Journal of geophysical
769 research, 69(24), 5181-5190.
770 Polnikov, V. G., (1993). On a description of a wind–wave energy dissipation function. In:
771 Donelan, M. A., Hui, W. H., Plant, W. J. (Eds.), The Air–sea Interface. Radio and
772 Acoustic Sensing, Turbulence and Wave Dynamics. Rosenstiel School of Marine and
773 Atmospheric Science, University of Miami, Miami, FL, 277-282.
774 Rogers, W. E., Babanin, A. V., and Wang, D. W. (2012). Observation-consistent input and
775 whitecapping dissipation in a model for wind-generated surface waves: Description
776 and simple calculations. Journal of Atmospheric and Oceanic Technology, 29(9),
777 1329-1346.
778 Sanders, J. W. (1976). A growth-stage scaling model for the wind-driven sea. Deutsche
779 Hydrografische Zeitschrift, 29(4), 136-161.

780 Snyder, R. L., Dobson, F. W., Elliott, J. A., and Long, R. B. (1981). Array measurements of
781 atmospheric pressure fluctuations above surface gravity waves. Journal of Fluid
782 mechanics, 102: 1-59.
783 Stewart, R. W. (1961). The wave drag of wind over water. Journal of fluid mechanics, 10(2),
784 189-194.
785 Stopa, J. E., Ardhuin, F., Babanin, A., and Zieger, S. (2016). Comparison and validation of
786 physical wave parameterizations in spectral wave models. Ocean Modelling, 103, 2-17.
787 The WAVEWATCH III R Development Group (WW3DG) (2016). User manual and system
788 documentation of WAVEWATCH III R version 5.16. Tech. Note 329,
789 NOAA/NWS/NCEP/MMAB, College Park, MD, USA, 326 pp. + Appendices.
790 Tolman, H. L. (2002). Validation of WAVEWATCH III version 1.15 for a global domain.
791 Technical Note, 213, 33.
792 Tolman, H. L., and Chalikov, D. (1996). Source terms in a third-generation wind wave
793 model. Journal of Physical Oceanography, 26(11), 2497-2518.
794 Wang, D. W., Mitchell, D. A., Teague, W. J., Jarosz, E., and Hulbert, M. S. (2005). Extreme
795 waves under hurricane Ivan. Science, 309(5736), 896-896.
796 Xu, Y., and Yu, X. (2020). Enhanced formulation of wind energy input into waves in
797 developing sea. Progress in Oceanography, 186, 102376.
798 Xu, Y., and Yu, X. (2021). Enhanced atmospheric wave boundary layer model for evaluation
799 of wind stress over waters of finite depth. Progress in Oceanography, 198, 102664.
800 Xu, Y., and Yu, X. (2022a): Enhanced Ocean Wave Modeling by Including Effect of
801 Breaking under Both Deep- and Shallow-Water Conditions – code files, Zenodo,
802 https://doi.org/10.5281/zenodo.7047221.
803 Xu, Y., and Yu, X. (2022b): Enhanced Ocean Wave Modeling by Including Effect of
804 Breaking under Both Deep- and Shallow-Water Conditions – input files of the
805 controlled normal condition cases, Zenodo, https://doi.org/10.5281/zenodo.7047234.
806 Xu, Y., and Yu, X. (2022c): Enhanced Ocean Wave Modeling by Including Effect of
807 Breaking under Both Deep- and Shallow-Water Conditions – input files of hurricane
808 Ivan case, Zenodo, https://doi.org/10.5281/zenodo.7047240.

809 Xu, Y., and Yu, X. (2022d): Enhanced Ocean Wave Modeling by Including Effect of
810 Breaking under Both Deep- and Shallow-Water Conditions – input files of hurricane
811 Katrina case, Zenodo, https://doi.org/10.5281/zenodo.7047244.
812 Young, I. R. (1999). Wind generated ocean waves. Elsevier.
813 Young, I. R., and Verhagen, L. A. (1996). The growth of fetch limited waves in water of
814 finite depth. Part 1. Total energy and peak frequency. Coastal Engineering, 29(1-2),
815 47-78.
816 Yuan, Y., Tung, C. C., and Huang, N. E. (1986). Statistical characteristics of breaking waves.
817 In: Phillips, O. M., Hasselmann, K. (Eds.), Wave Dynamics and Radio Probing of the
818 Ocean Surface. Plenum Press, New York, 265-272.
819 Zakharov, V. E., Resio, D., and Pushkarev, A. (2012). New wind input term consistent with
820 experimental, theoretical and numerical considerations. arXiv preprint
821 arXiv:1212.1069.
822 Zakharov, V., Resio, D., and Pushkarev, A. (2017). Balanced source terms for wave
823 generation within the Hasselmann equation. Nonlinear Processes in Geophysics, 24(4),
824 581-597.
825 Zieger, S., Babanin, A. V., Rogers, W. E., and Young, I. R. (2015). Observation-based source
826 terms in the third-generation wave model WAVEWATCH. Ocean Modelling, 96, 2-25.
827